the MLO family in a tissue-specific manner. The ancestral function of FER and MLO proteins is an open question, but the presence of genes with high sequence-relatedness to *FER* and *MLO* in bryophytes (*27*, *28*) suggests that these proteins were either originally implicated in processes distinct from PT reception and PM susceptibility, or that their cooperativity developed later in the course of evolution. As both proteins are required for compatible interactions with either PTs or fungal hyphae, their original role may have been in mediating susceptibility to symbiotic organisms such as mycorrhizal fungi, an interaction that was important for land plant evolution but no longer occurs with *Arabidopsis*. Because *FER* is necessary for successful fertilization, deleterious mutations that would also lead to PM resistance would be selected against. Other players in PT reception (*29*, *30*) may also be involved in PM infection, or, alternatively, different accessory molecules may be used in conjunction with FER and the MLOs in distinct response pathways.

Successful seed production and durable resistance to pathogens are two of the most important agronomic traits sought after today. The work presented here has unveiled unforeseen similarities between these processes at the molecular level. As we continue to unravel the signal transduction processes involved in intercellular communication during PT reception, we may also gain important insights into PM resistance mechanisms and vice versa.

References and Notes

1. E. M. Lord, S. D. Russell, *Annu. Rev. Cell Dev. Biol.* **18**, 81 (2002).
2. J. B. Amici, *Annales des Sciences Naturelles*, 193 (1847).
3. T. Dresselhaus, *Curr. Opin. Plant Biol.* **9**, 41 (2006).
4. S. Okuda *et al.*, *Nature* **458**, 357 (2009).
5. L. Sandaklie-Nikolova, R. Palanivelu, E. J. King, G. P. Copenhaver, G. N. Drews, *Plant Physiol.* **144**, 1753 (2007).
6. N. Huck, J. M. Moore, M. Federer, U. Grossniklaus, *Development* **130**, 2149 (2003).
7. N. Rotman *et al.*, *Curr. Biol.* **13**, 432 (2003).
8. J. M. Escobar-Restrepo *et al.*, *Science* **317**, 656 (2007).
9. T. Livius, *Ab Urbe Condita, Liber VII, 3.7* (~29 B.C.).
10. R. Büschges *et al.*, *Cell* **88**, 695 (1997).
11. Z. Chen *et al.*, *Plant Mol. Biol.* **60**, 583 (2006).
12. C. Consonni *et al.*, *Nat. Genet.* **38**, 716 (2006).
13. Z. Chen *et al.*, *Plant Cell* **21**, 1972 (2009).
14. S. E. Wuest *et al.*, *Curr. Biol.* **20**, 506 (2010).
15. R. A. Bhat, M. Miklis, E. Schmelzer, P. Schulze-Lefert, R. Panstruga, *Proc. Natl. Acad. Sci. U.S.A.* **102**, 3135 (2005).
16. T. Higashiyama, *J. Plant Res.* **115**, 149 (2002).
17. K. Amano, *Host Range and Geographical Distribution of the Powdery Mildew Fungi* (Japan Scientific Societies Press, Tokyo, 1986).
18. J. D. Jones, J. L. Dangl, *Nature* **444**, 323 (2006).
19. P. Piffanelli *et al.*, *Nature* **430**, 887 (2004).
20. K. H. Wolfe, M. Gouy, Y. W. Yang, P. M. Sharp, W. H. Li, *Proc. Natl. Acad. Sci. U.S.A.* **86**, 6201 (1989).
21. H. Guo *et al.*, *Proc. Natl. Acad. Sci. U.S.A.* **106**, 7648 (2009).
22. R. J. O'Connell, R. Panstruga, *New Phytol.* **171**, 699 (2006).
23. R. Bari, J. D. Jones, *Plant Mol. Biol.* **69**, 473 (2009).
24. P. Piffanelli *et al.*, *Plant Physiol.* **129**, 1076 (2002).
25. R. Panstruga, *Biochem. Soc. Trans.* **33**, 389 (2005).
26. S. Amien *et al.*, *PLoS Biol.* **8**, e1000388 (2010).
27. A. Devoto *et al.*, *J. Mol. Evol.* **56**, 77 (2003).
28. M. D. Lehti-Shiu, C. Zou, K. Hanada, S. H. Shiu, *Plant Physiol.* **150**, 12 (2009).
29. A. Capron *et al.*, *Plant Cell* **20**, 3038 (2008).
30. A. Boisson-Dernier, S. Frietsch, T. H. Kim, M. B. Dizon, J. I. Schroeder, *Curr. Biol.* **18**, 63 (2008).

31. We thank A. Boisson-Dernier for providing *pLat52:DsRED* and for critical reading of this manuscript; S. Schauer for providing plasmids; A. Reinstädler for technical assistance with pathogen assays; and J. M. Escobar-Restrepo, H. Lindner, M. Bayer, C. Jäger-Baroux, S. Pien, V. Gagliardini, and members of the Grossniklaus lab for helpful discussions. This work was supported by the University of Zürich, the Max Planck Society, fellowships of the Human Frontiers in Science Program (to S.A.K.), the Forschungskredit of the University of Zürich (to H.S.-A.), the International Max Planck Research School (to N.F.K.), the Royal Society of London (to G.I.), and grants from the Deutsche Forschungsgemeinschaft (SFB670 to R.P.) and the Swiss National Science Foundation (to U.G.).

Supporting Online Material

www.sciencemag.org/cgi/content/full/330/6006/968/DC1
Materials and Methods
SOM Text
Figs. S1 to S11
Tables S1 to S3
References

16 July 2010; accepted 15 September 2010
10.1126/science.1195211

Optogenetic Control of Cardiac Function

Aristides B. Arrenberg,[1,3] Didier Y. R. Stainier,[2]* Herwig Baier,[1] Jan Huisken[2,4]

The cardiac pacemaker controls the rhythmicity of heart contractions and can be substituted by a battery-operated device as a last resort. We created a genetically encoded, optically controlled pacemaker by expressing halorhodopsin and channelrhodopsin in zebrafish cardiomyocytes. Using patterned illumination in a selective plane illumination microscope, we located the pacemaker and simulated tachycardia, bradycardia, atrioventricular blocks, and cardiac arrest. The pacemaker converges to the sinoatrial region during development and comprises fewer than a dozen cells by the time the heart loops. Perturbation of the activity of these cells was entirely reversible, demonstrating the resilience of the endogenous pacemaker. Our studies combine optogenetics and light-sheet microscopy to reveal the emergence of organ function during development.

In mammals, the heart rate is controlled by a specialized group of cells in the sinoatrial (SA) node, which act as the primary pacemaker. Together with cells in the atrioventricular (AV) node (secondary pacemaker) and specialized cells in the ventricular walls, they constitute the cardiac conduction system (CCS) (*1*, *2*). In nonmammalian vertebrates, a CCS with properties similar to those of the mammalian CCS has been inferred from imaging of voltage signals (*3*, *4*) or Ca^{2+} transients (*5*); the origin of the conduction wave was located in a region apparently homologous to the SA node. However, the exact role of this presumptive pacemaker and the consequences of its inactivation remain unclear.

We combined optical tools and transgenic expression of light-gated ion channels (*6*–*8*) in zebrafish (*9*–*13*) to locate and control cardiac pacemaker cells. Halorhodopsin (NpHR) (*6*) and channelrhodopsin-2 H134R (ChR2) (*6*, *14*) enable temporally precise (tens of milliseconds) and spatially confined (single cells) control. The light-gated pump NpHR-mCherry was expressed in zebrafish cardiomyocytes by means of the Gal4/UAS system (*13*, *15*) (fig. S1A). The protein was locally activated with light patterns generated with a digital micromirror device (fig. S2), which enables synchronous, uniform illumination of arbitrary shapes, unlike laser scanning (*16*) or fiber optic (*13*) techniques. High-speed video recordings of the heart were generated with a multidirectional selective plane illumination microscope (mSPIM) (*17*–*19*) (Fig. 1A and fig. S3).

Illuminating the entire zebrafish heart at 3 days post-fertilization (dpf) with orange light instantaneously blocked contractions (Fig. 1B and movie S1), indicating that the strong hyperpolarization induced by the activated chloride pump NpHR perturbed the well-balanced interplay of ion channels in cardiomyocytes (fig. S1B) and prevented depolarizations. The heart recovered to its original beat rate instantaneously after cessation of illumination [in zebrafish, blood circulation is dispensable for survival up to 6 dpf (*20*)].

We observed that the sinoatrial region was more susceptible to NpHR manipulation than the working myocardium in the atrium and ventricle, most likely because the current densities across the cell membranes of CCS cells are smaller by a factor of >10 (*21*, *22*). To locate the pacemakers in a nonbiased way, we sequentially illuminated small, overlapping regions with constant intensity (Fig. 1C and movie S2). Maps showing the heart rate for every illuminated area were generated (Fig. 1D and fig. S4) to identify regions in which NpHR activation induced cardiac arrest or

[1]Department of Physiology, University of California, San Francisco, CA 94158, USA. [2]Department of Biochemistry and Biophysics and Cardiovascular Research Institute, University of California, San Francisco, CA 94158, USA. [3]Institute of Biology 1, University of Freiburg, 79104 Freiburg, Germany. [4]Max Planck Institute of Molecular Cell Biology and Genetics, 01307 Dresden, Germany.

*To whom correspondence should be addressed. E-mail: didier.stainier@ucsf.edu

ventricular arrhythmia. Pattern generation, data recording, and video analysis were automated and computer-controlled to enable fast and reproducible analysis of a large number of hearts (*23*).

To follow the maturation of the CCS over embryonic and larval development, we generated heart rate maps for five stages (1 dpf to 5 dpf; n = 3 to 15 hearts analyzed, mean 7.4 per stage) from different angles. In 1-dpf animals, the heart stopped beating when a large region at the venous pole of the heart was illuminated at medium light intensities (Fig. 2A). At higher light intensities, it was possible to block the heartbeat by illuminating different smaller patches of the venous pole (fig. S5A). This observation indicates that strong electrical coupling seemed to be present and suggests that at this stage the cells required to initiate the heartbeat (pacemaker cells) cover a large area at the venous pole.

In 2-dpf animals, the pacemaker region was more confined to the sinoatrial ring (SAR; Fig. 2B and fig. S5B). Although no consistent bias was found, individual hearts were more easily arrested by illuminating the right part of the SAR (right-biased: 8 hearts, left-biased: 5 hearts). Illumination of large areas adjacent to the pacemaker region did not arrest the heart (movies S3 to S5), indicating that the silencing effect did not spread farther than one or two cell diameters outside the illuminated area.

The atrioventricular canal (AVC) is formed at 2 dpf (*24*). At this stage, AV blocks were induced with high illumination intensities at the AVC; from 3 to 5 dpf, lower light intensities were sufficient to block ventricular systoles. No bias was detected around the AVC perimeter, which suggests that all AVC cells contribute equally to the conduction of the beat from the atrium to the ventricle. It has been shown that upon ablation of the primary pacemaker, downstream pacemakers such as the AV node can take over to maintain heartbeat (*25*). In our experiments, beating was always blocked when the SAR was silenced; this result implies that pacemaker currents outside the SAR are not strong enough to drive the larval heart immediately after SAR silencing.

The pacemaker region became further defined at 3 dpf (Fig. 2C and fig. S5C). The cells required to initiate the heartbeat were confined to the dorsal right quadrant of the SAR in 10 of the 13 hearts investigated, as revealed by mapping the heart from different angles. A refinement of the pacemaker area during development has also been reported in other species, where it narrows to a small region as it migrates from the atria to the right sinus primordium (*3*). In amniotes, the pacemaker is generally situated on the right side, which matches our findings in zebrafish. Furthermore, the center of the region appeared to be located about 10 μm (one or two cell diameters) farther anterior than the neck of the SAR (Fig. 2D). Interestingly, the cells that make up the lips of the sinus adjacent to the SAR appear to have an intrinsic pacemaking capability and poor coupling to the SAR, because they continued to contract in the arrested heart (movie S6), and photosilencing their contractions did not arrest the heart. The number of cells required for beating varied between animals. The size of the illuminated area generally corresponded to 10 to 30 cells, but some hearts could be arrested by illuminating very few cells (3 cells, movies S7 and S8). At 4 and 5 dpf, the pacemaker cells remained at the same relative position (Fig. 2, D and E, and fig. S5, D and E).

The zebrafish heart can be manipulated very precisely to rapidly switch between a healthy and a diseased state. We generated prominent cardiac pathologies such as AV blocks, tachycardia, and bradycardia. When illuminating the AVC (Fig. 3A), we induced different AV blocks by varying the light intensity. At high intensities, 3:1 or 4:1 AV blocks could be induced (Fig. 3, B and C); medium intensities caused 2:1 AV blocks (movie S9). Notably, the 2:1 AV block was stable over a

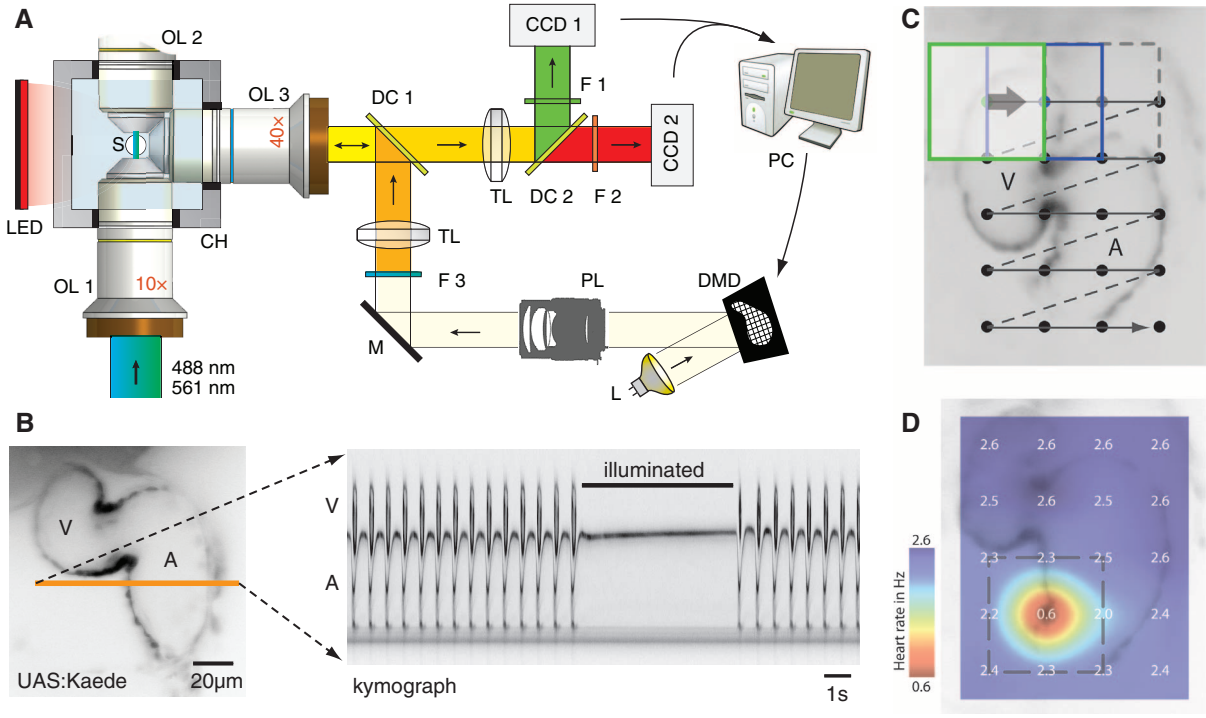

Fig. 1. Automated mapping of the cardiac pacemaker using patterned illumination in an mSPIM. (**A**) Microscope layout. A sheet of laser light (488 nm or 561 nm) illuminates the embedded fish (S) through objective lens OL1 or OL2. A computer-generated pattern is reflected off the digital micromirror device (DMD) and imaged onto the sample (S) through the detection lens OL3. See fig. S3 for details. LED, light-emitting diode (transmission); CH, chamber; DC, dichroic mirror; TL, tube lens; F, filter; M, mirror; PL, photographic lens; L, light bulb; CCD, charge-coupled device (camera). (**B**) A 3-dpf zebrafish heart expressing NpHR-mCherry stopped beating when illuminated with orange light and recovered instantaneously afterward. A high-speed video of an optical section was obtained by low-intensity light-sheet illumination. The kymograph shows the motion of the heart wall along the highlighted line. V, ventricle; A, atrium. The animal was transgenic for *Et(E1b:Gal4-VP16)s1101t*, *Tg(UAS:NpHR-mCherry)s1989t*, and *Tg(UAS:Kaede)s1999t*. Dark coloration corresponds to high Kaede fluorescence (inverted image). See movie S1. (**C**) The whole heart was sequentially illuminated with overlapping squares (see movie S2). (**D**) False-color image of the observed atrial heart rate after illumination of 20 sampled areas (ventral view, with head pointing upward). In this 3-dpf fish, the pacemaker cells are located in the dorsal-right side of the inflow ring.

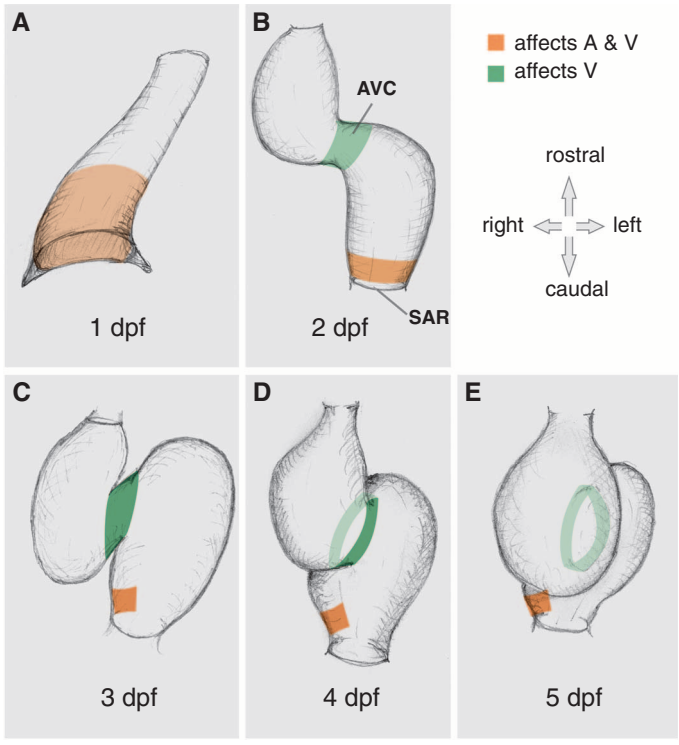

Fig. 2. Localization of the areas sensitive to hyperpolarization at the inflow and atrioventricular canal (AVC) regions of 1- to 5-dpf hearts. (**A** to **E**) Schematic drawings of the pacemaker (red) and AVC (green) regions for the developmental stages indicated SAR, sinoatrial region.

range of intensities (55 to 95% maximal light intensity; see vertical lines in Fig. 3C) and for prolonged periods of time (50 s; Fig. 3C). The induction of different AV blocks was reproducible in many different hearts (Fig. 3D), although the required light intensity varied between hearts, probably because of the varying expression levels of NpHR. In some hearts, a complete block of ventricular beats could be produced with high light intensities (movie S9).

Periodic photoactivation of the SAR with ChR2 (Fig. 3E) was used to control the heart rate in 4-dpf animals within the frequency range 2.7 to 4.7 Hz (Fig. 3F; heart rate before perturbation was 3.3 Hz). Above 4.7 Hz, atrial contractions started to skip pulses and became variable, suggesting that the heart rate cannot be sustained at such high frequency. Interestingly, our method enabled a reduction in heart rate, a modulation that was not reported in a recent study using a different laser-based stimulation technique (*26*).

In vertebrate hearts, the conduction direction is determined by the beating rates of primary (faster) and downstream (slower) pacemakers. Retrograde excitation has been reported in the zebrafish heart (*27*), and we were interested to know whether it could be forced to beat regularly in the retrograde

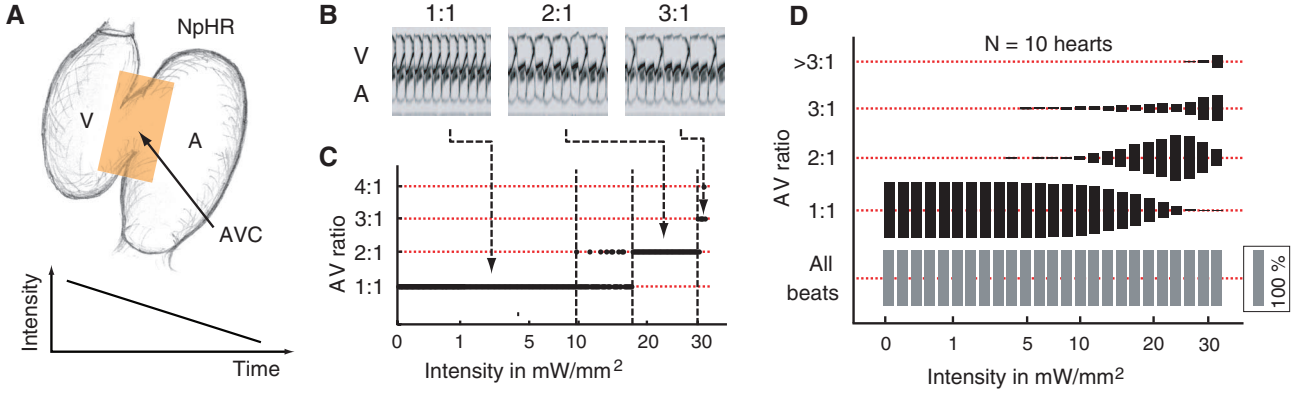

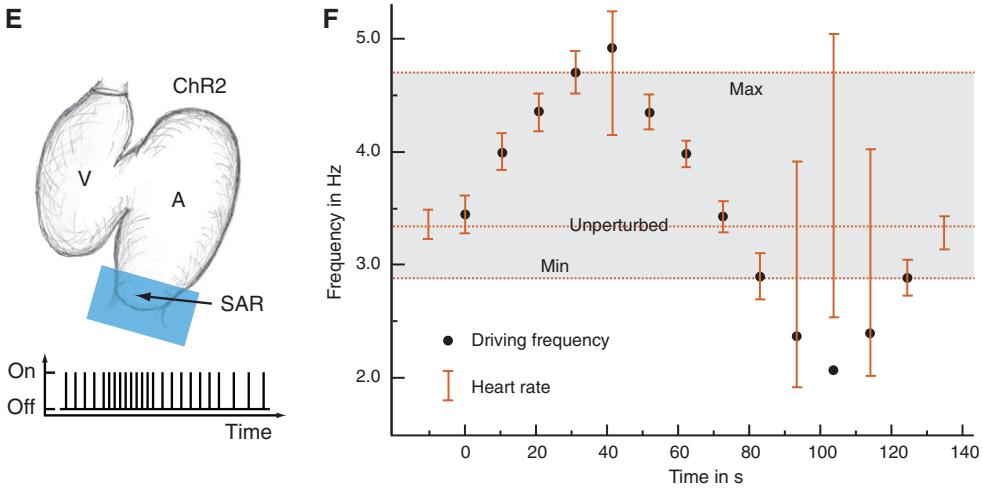

Fig. 3. Optically induced atrioventricular arrhythmia, tachycardia, and bradycardia. (**A** to **D**) Ventricular blocks of different severity are induced by illuminating the AVC with well-defined intensities. (A) Schematic of the spatial and temporal pattern of illumination. The atrioventricular ring in NpHR-expressing hearts was illuminated with slowly decreasing intensity. (B) Kymograph and (C) AV ratio for different illumination intensities. High intensities induced a 3:1 block, medium intensities a 2:1 block. (D) Summary for 10 different hearts. See movie S9. (**E**) Schematic of the region and temporal pattern of illumination. The sinoatrial ring in ChR2 expressing hearts was illuminated with short pulses with varying frequency. (**F**) The heart rate (brown bars) relative to the driving frequency (black dots) during the course of the experiment. The heart rate followed the driving frequency within the indicated dynamic range (between Min and Max). Error bars represent SD. See movie S10. A, atrium; V, ventricle; AVC, atrioventricular canal; SAR, sinoatrial ring.

direction. We applied light pulses to a ventricular region close to the bulbus to rhythmically activate ChR2 and found that cardiac conduction could be reversed (movie S11 and fig. S6) for at least 30 consecutive heartbeats.

Our results show that a surprisingly small number of pacemaker cells is indispensable for heartbeat initiation. This makes the embryonic heart very vulnerable, as no compensating mechanism seems to be in place on the time scales observed. Moreover, we have shown that this area can be optically targeted; our photostimulation methods allowed us to optically control heart rate, reverse cardiac conduction, and induce disease-like states in a reversible manner. This work opens a new avenue for controlling hemodynamic forces during studies on epigenetic factors of heart formation (*28*) and blood vessel development (*29*).

References and Notes

1. T. Mikawa, R. Hurtado, *Semin. Cell Dev. Biol.* **18**, 90 (2007).
2. M. R. Jongbloed, E. A. Mahtab, N. A. Blom, M. J. Schalij, A. C. Gittenberger-de Groot, *ScientificWorldJournal* **8**, 239 (2008).
3. K. Kamino, A. Hirota, S. Fujii, *Nature* **290**, 595 (1981).
4. D. Sedmera *et al.*, *Am. J. Physiol. Heart Circ. Physiol.* **284**, H1152 (2003).
5. N. C. Chi *et al.*, *PLoS Biol.* **6**, e109 (2008).
6. F. Zhang *et al.*, *Nature* **446**, 633 (2007).
7. M. Scanziani, M. Häusser, *Nature* **461**, 930 (2009).
8. L. Luo, E. M. Callaway, K. Svoboda, *Neuron* **57**, 634 (2008).
9. A. D. Douglass, S. Kraves, K. Deisseroth, A. F. Schier, F. Engert, *Curr. Biol.* **18**, 1133 (2008).
10. S. Szobota *et al.*, *Neuron* **54**, 535 (2007).
11. C. Wyart *et al.*, *Nature* **461**, 407 (2009).
12. H. Baier, E. K. Scott, *Curr. Opin. Neurobiol.* **19**, 553 (2009).
13. A. B. Arrenberg, F. Del Bene, H. Baier, *Proc. Natl. Acad. Sci. U.S.A.* **106**, 17968 (2009).
14. G. Nagel *et al.*, *Proc. Natl. Acad. Sci. U.S.A.* **100**, 13940 (2003).
15. E. K. Scott *et al.*, *Nat. Methods* **4**, 323 (2007).
16. O. G. Ayling, T. C. Harrison, J. D. Boyd, A. Goroshkov, T. H. Murphy, *Nat. Methods* **6**, 219 (2009).
17. J. Huisken, J. Swoger, F. Del Bene, J. Wittbrodt, E. H. Stelzer, *Science* **305**, 1007 (2004).
18. P. J. Scherz, J. Huisken, P. Sahai-Hernandez, D. Y. Stainier, *Development* **135**, 1179 (2008).
19. J. Huisken, D. Y. Stainier, *Opt. Lett.* **32**, 2608 (2007).
20. A. J. Sehnert *et al.*, *Nat. Genet.* **31**, 106 (2002).
21. R. Wilders, *Conf. Proc. IEEE Eng. Med. Biol. Soc.* **2007**, 152 (2007).
22. A. Nygren *et al.*, *Circ. Res.* **82**, 63 (1998).
23. See supporting material on *Science* Online.
24. D. Beis *et al.*, *Development* **132**, 4193 (2005).
25. D. Scherf, *Z. Gesamte Exp. Med.* **57**, 188 (1927).
26. M. W. Jenkins *et al.*, *Nat. Photonics* **4**, 623 (2010).
27. D. J. Milan, A. C. Giokas, F. C. Serluca, R. T. Peterson, C. A. MacRae, *Development* **133**, 1125 (2006).
28. J. R. Hove *et al.*, *Nature* **421**, 172 (2003).
29. C. Hahn, M. A. Schwartz, *Nat. Rev. Mol. Cell Biol.* **10**, 53 (2009).

30. We thank T. Mikawa, R. Shaw, and A. Müssigbrodt for feedback and comments on the manuscript. Supported by NIH grant HL54737 (D.Y.R.S.), the Packard Foundation (D.Y.R.S.), NIH grant R01 NS053358 (H.B.), a Sandler Opportunity Award, the Byers Award for Basic Science (H.B.), and the NIH Nanomedicine Development Center "Optical Control of Biological Functions" (H.B.). J.H. was supported by a Human Frontier Science Program (HFSP) cross-disciplinary fellowship. A.B.A. was supported by a Boehringer Ingelheim Fonds (B.I.F.) and a Krevans fellowship. The optogenetic idea, transgenic lines, and original observation originated in H.B.'s lab; follow-up experiments were carried out in D.Y.R.S.'s lab as an equal collaboration between A.B.A. and J.H. All authors worked on the manuscript, which was drafted by A.B.A. and J.H.

Supporting Online Material

www.sciencemag.org/cgi/content/full/330/6006/971/DC1
Materials and Methods
Figs. S1 to S7
Movies S1 to S11

2 August 2010; accepted 1 October 2010
10.1126/science.1195929

Kinetic Scaffolding Mediated by a Phospholipase C–β and G_q Signaling Complex

Gary L. Waldo,[1] Tiffany K. Ricks,[1] Stephanie N. Hicks,[1] Matthew L. Cheever,[1] Takeharu Kawano,[2] Kazuhito Tsuboi,[2] Xiaoyue Wang,[3] Craig Montell,[3] Tohru Kozasa,[2,4] John Sondek,[1,5,6] T. Kendall Harden[1,6]*

Transmembrane signals initiated by a broad range of extracellular stimuli converge on nodes that regulate phospholipase C (PLC)–dependent inositol lipid hydrolysis for signal propagation. We describe how heterotrimeric guanine nucleotide–binding proteins (G proteins) activate PLC-βs and in turn are deactivated by these downstream effectors. The 2.7-angstrom structure of PLC-β3 bound to activated $G\alpha_q$ reveals a conserved module found within PLC-βs and other effectors optimized for rapid engagement of activated G proteins. The active site of PLC-β3 in the complex is occluded by an intramolecular plug that is likely removed upon G protein–dependent anchoring and orientation of the lipase at membrane surfaces. A second domain of PLC-β3 subsequently accelerates guanosine triphosphate hydrolysis by $G\alpha_q$, causing the complex to dissociate and terminate signal propagation. Mutations within this domain dramatically delay signal termination in vitro and in vivo. Consequently, this work suggests a dynamic catch-and-release mechanism used to sharpen spatiotemporal signals mediated by diverse sensory inputs.

Phospholipase C (PLC) catalyzes the hydrolysis of phosphatidylinositol 4,5-bisphosphate [PtdIns(4,5)P_2] to the second messengers inositol 1,4,5-trisphosphate [Ins(1,4,5)P_3] and diacylglycerol in an essential step for the physiological action of many hormones, neurotransmitters, growth factors, and other extracellular stimuli (*1*–*3*). These cascades use signaling complexes consisting of Gα subunits of the G_q family ($G\alpha_q$, 11, 14, and 16) of heterotrimeric guanine nucleotide–binding proteins (G proteins) and PLC-β isozymes (β1-4) (*4*–*6*). Agonist-stimulated receptors increase exchange of guanosine triphosphate (GTP) for guanosine diphosphate (GDP) on $G\alpha_q$, GTP-bound $G\alpha_q$ engages and activates PLC-β, and PLC-β increases up to three orders of magnitude the rate of hydrolysis of GTP by its activating G protein (*7*–*9*). Coordination from upstream and downstream inputs sharpens time frame, amplitude, and on-off cycling of these signaling nodes. Although kinetic analyses revealed much about the dynamics of $G\alpha_q$/PLC-β signaling complexes (*10*–*12*), how PLC-βs simultaneously act as effectors and GTPase activating proteins (GAPs) has remained unknown. Here, we describe the structure of PLC-β3 in an activated complex with $G\alpha_q$, which together with supporting biochemical and physiological analyses reveals its mechanism of transmembrane signaling.

The three-dimensional structure of an AlF_4^--dependent complex of $G\alpha_q$ bound to PLC-β3 was solved by molecular replacement using PLC-β2 [Protein Data Bank (PDB) code 2FJU] and $G\alpha_q$ (PDB 2BCJ) as search models and refined at 2.7-Å resolution (table S1). PLC-β3 engages $G\alpha_q$ through three distinct regions (Fig. 1, A and B). First, an extended loop between the third and fourth EF hands of PLC-β3 directly buttresses switch residues critical for GTP hydrolysis by $G\alpha_q$. Second, the region of PLC-β3 that connects the catalytic TIM barrel and the C2 domain interacts with both switches 1 and 2 of $G\alpha_q$. Third, a segment composed of a helix-turn-helix at the C terminus of the C2 domain resides primarily within a shallow declivity on the surface of $G\alpha_q$ formed by switch 2 and α3. Other effectors are known to engage this region within Gα subunits (Fig. 1C). GTP hydrolysis by Gα subunits is independently accelerated by a large family of regulator of G protein signaling (RGS) proteins (*8*, *13*, *14*), and PLC-β3 interacts with a surface on $G\alpha_q$ that overlaps almost completely with portions of Gα subunits needed for engagement of RGS proteins (Fig. 1C). Consistent with a biologically relevant interface (*15*), the complex

[1]Department of Pharmacology, University of North Carolina School of Medicine, Chapel Hill, NC 27599, USA. [2]Department of Pharmacology, University of Illinois, Chicago, IL 60612, USA. [3]Departments of Biological Chemistry and Neuroscience, Center for Sensory Biology, Johns Hopkins University School of Medicine, Baltimore, MD 21205, USA. [4]Laboratory for Systems Biology and Medicine, Research Center for Advanced Science and Technology, University of Tokyo, Tokyo 153-8904, Japan. [5]Department of Biochemistry, University of North Carolina School of Medicine, Chapel Hill, NC 27599, USA. [6]Lineberger Cancer Center, University of North Carolina School of Medicine, Chapel Hill, NC 27599, USA.

*To whom correspondence should be addressed. E-mail: tkh@med.unc.edu